ACS Macro Letters

Letter

pubs.acs.org/macroletters

Dual-Spun Shape Memory Elastomeric Composites

Jaimee M. Robertson, Hossein Birjandi Nejad, and Patrick T. Mather*

Syracuse Biomaterials Institute and Biomedical and Chemical Engineering Department, Syracuse University, Syracuse, New York 13244, United States

Supporting Information

ABSTRACT: Thermally responsive shape memory polymers (SMPs) are typically relatively stiff due to the need to vitrify the polymer chains to fix a temporary shape. A need exists for elastomeric SMPs with mechanical properties that more closely match those of human tissue. In this communication, we present a novel approach to fabricate a fully thermoplastic elastomeric SMP. Two polymers are simultaneously electrospun, or dual-spun, forming a composite fiber mat with a controllable composition. The two polymers were chosen such that one assists in "shape fixing" and the other in "shape recovery". We envision that the versatility and simplicity of this fabrication approach will allow for large scale production of shape memory elastomeric composites (SMECs) for a wide range of applications.

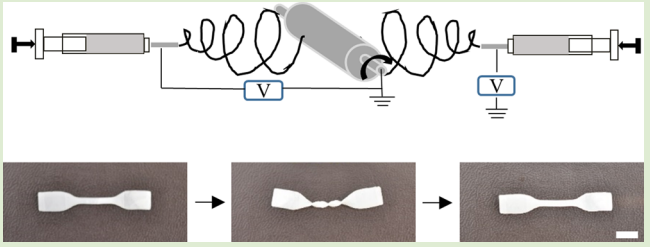

Shape memory polymers (SMPs) constitute a unique class of polymers that have the ability to fix a temporary shape until they are triggered to return to their original form by an external stimulus.[1,2] The stimulus activating the shape changing mechanism can be heat,[3−6] solvent,[7−9] electrical current,[10,11] light,[12−14] magnetic fields,[15−17] or a change in pH.[18,19] By far, heat-triggered SMPs is the subclass that has been studied in the most depth.[2] The shape changing mechanism is performed around a transition temperature, often a glass transition temperature (T_g), and relies on vitrification of the chains upon cooling to fix the temporary shape.[20] Consequently, SMPs in their fixed state are relatively stiff. A need exists for soft, extensible SMPs with mechanical properties that more closely match those of human tissue. Our group has previously introduced a shape memory elastomeric composite (SMEC) that is rubbery and soft and, yet, has the ability to fix a temporary shape.[21] In this case, the SMP is above its T_g at room temperature (RT), resulting in a lower modulus, and the shape memory (SM) is performed around the SMP's melting point (T_m). However, the utilized processing techniques introduce limitations on the SMEC's production at a larger scale due to the multistep fabrication method, which requires up to several days. Our current work presents a simple strategy to prepare SMECs more efficiently and with more control over the composition, thus allowing for adjustment of material properties to meet requirements of a variety of applications.

In this communication, we introduce a fully thermoplastic SMEC prepared by dual-electrospinning[22,23] and compression molding. Solutions of poly(ε-caprolactone) (PCL) and Pellethane 5863−80A (hereafter, "Pellethane"; a polyether-based thermoplastic polyurethane elastomer[24]) were prepared separately and were simultaneously electrospun onto a rotating mandrel from opposite sides of the mandrel. A schematic of the dual-electrospinning setup is shown in Figure 1a. The resulting composite fiber mats contained interspersed fibers (Figure 1c) of both polymers, with varying PCL weight fractions. After drying in a vacuum oven at RT overnight, the composite fibers were compression molded into films (Figure 1d) at 80 °C to obtain nonporous, homogeneously distributed films. This temperature was chosen such that it was above the melting temperature (T_m) of PCL (56 °C), but below the T_m of Pellethane (157 °C; Figure 2). The resulting morphology contains Pellethane fibers within a PCL matrix (Figure 1b).

Differential scanning calorimetry (DSC) was utilized to estimate the weight fraction of PCL in the composites. A comparison of the second heating cycles of the SMECs to those of neat PCL and Pellethane (Figure 2) revealed that the transitions of both components are found in the composites, and the transition temperatures are unchanged, indicating that the components remain in discrete phases. This was further supported by a microstructural analysis, in which wide-angle X-ray scattering (WAXS) was employed, with results indicating that the crystalline *d*-spacings were unaltered in the SMECs (a more detailed WAXS analysis is provided in the Supporting Information). The PCL weight fraction in the composite was measured as the ratio of the heat of melting of PCL in the SMEC to the heat of melting of neat PCL. These values, reported as weight percentages (wt %), were very close to the nominal PCL weight fractions and were used to characterize the SMECs throughout this communication. The measured PCL content ranged from 2 to 31 wt % PCL for the prepared SMECs.

Dynamic mechanical analysis (DMA) was performed on the SMECs and the individual components (Figure 3) to compare

Received: February 9, 2015
Accepted: March 30, 2015
Published: April 1, 2015

DOI: 10.1021/acsmacrolett.5b00106
ACS Macro Lett. 2015, 4, 436−440

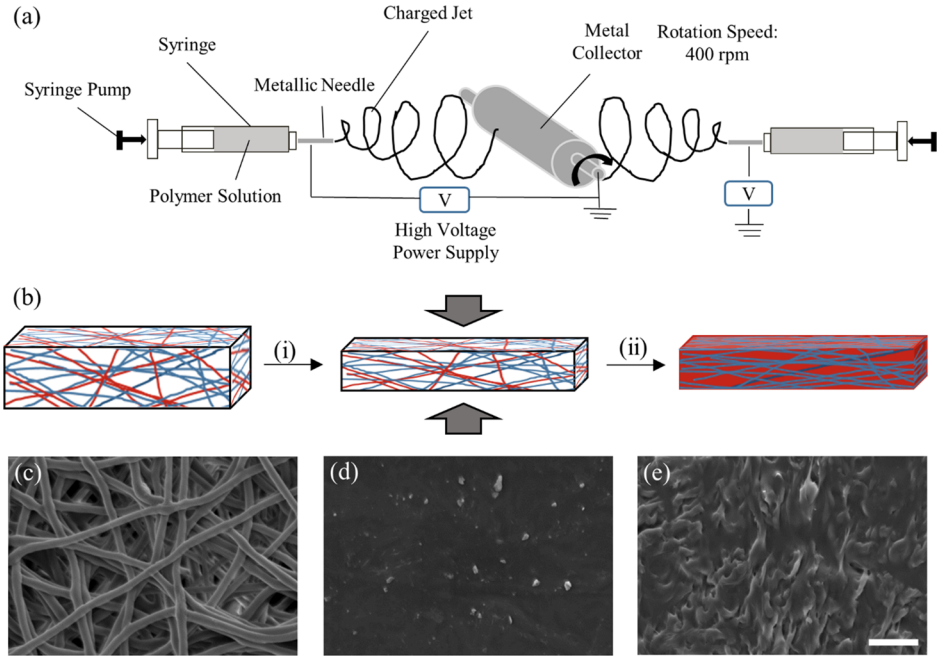

Figure 1. Dual-spun shape memory elastomeric composite (SMEC) preparation. (a) Schematic showing the dual-electrospinning setup, which contains two syringes holding different polymer solutions placed on opposing sides of the collector drum. The polymers are simultaneously electrospun, or dual-spun, forming composite mats. (b) The composite fiber mats with PCL (red) and Pellethane (blue) fibers are (i) compacted with 1 metric ton force and (ii) heated (in the compacted state) to 80 °C to melt the PCL fibers and form a SMEC film with Pellethane fibers contained within a PCL matrix. Representative scanning electron microscopy (SEM) images of (c) dual-spun fibers, (d) the surface of a compression molded SMEC film, and (e) the cross-section of a SMEC film. SEM images of all SMEC compositions are available in the Supporting Information. The scale bar represents 10 μm for all SEM images.

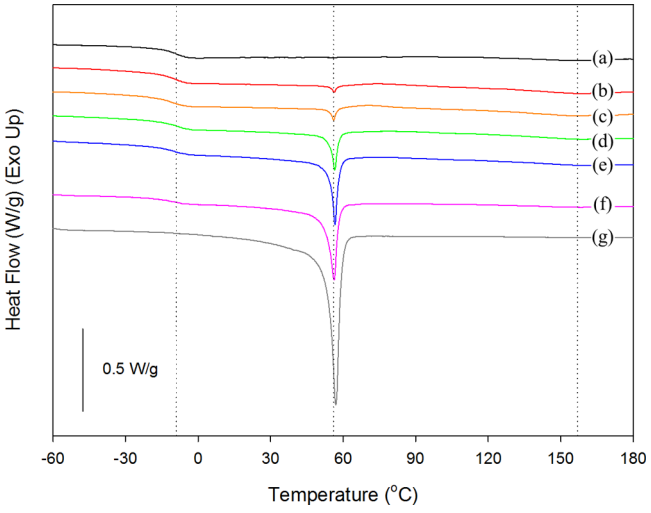

Figure 2. Differential scanning calorimetry second heating curves of SMECs with (a) 0 (neat Pellethane), (b) 2, (c) 5, (d) 16, (e) 26, (f) 31, and (g) 100 (neat PCL) wt % PCL (heating and cooling rates were 10 °C min^{-1}). The SMECs exhibit the transitions of both the PCL and the Pellethane. From left to right, the vertical dotted lines represent Pellethane's T_g (−9 °C), PCL's T_m (56 °C), and Pellethane's T_m (157 °C). The heat of melting of the PCL crystalline phase increases with increasing PCL content. The weight fraction of PCL in the SMEC was calculated by dividing the heat of melting of the PCL phase in the SMEC by the heat of melting of neat PCL. The DSC second heating curve for neat Pellethane is available in the Supporting Information to better expose the melting transition at 157 °C.

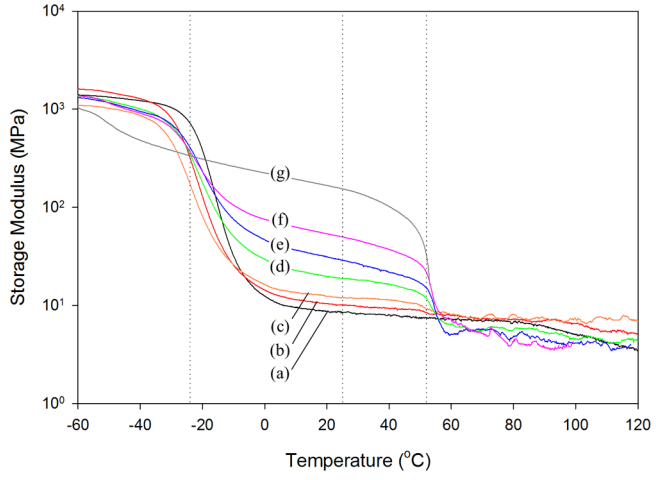

Figure 3. Dynamic mechanical analysis of SMECs with (a) 0 (neat Pellethane), (b) 2, (c) 5, (d) 16, (e) 26, (f) 31, and (g) 100 (neat PCL) wt % PCL. The SMECs exhibit storage moduli between those of PCL and Pellethane, and the RT storage modulus increases with increasing PCL content. From left to right, the vertical dotted lines represent the onset (−24 °C) of modulus drop due to Pellethane's T_g, RT (25 °C), and the onset (52 °C) of modulus drop due to PCL's T_m. A summary of the thermomechanical properties is provided in the Supporting Information.

the thermomechanical properties, anticipating relevance to shape memory properties studied later (loss tangent curves are available in the Supporting Information). The Pellethane and SMECs showed a drop in storage modulus around −20 °C due to the T_g of Pellethane. Notably, the storage moduli of the SMECs are between that of the individual components in the −10 to 50 °C range. Further, in this region, there is a trend of increasing modulus with increasing PCL content. Specifically, at

DOI: 10.1021/acsmacrolett.5b00106
ACS Macro Lett. 2015, 4, 436−440

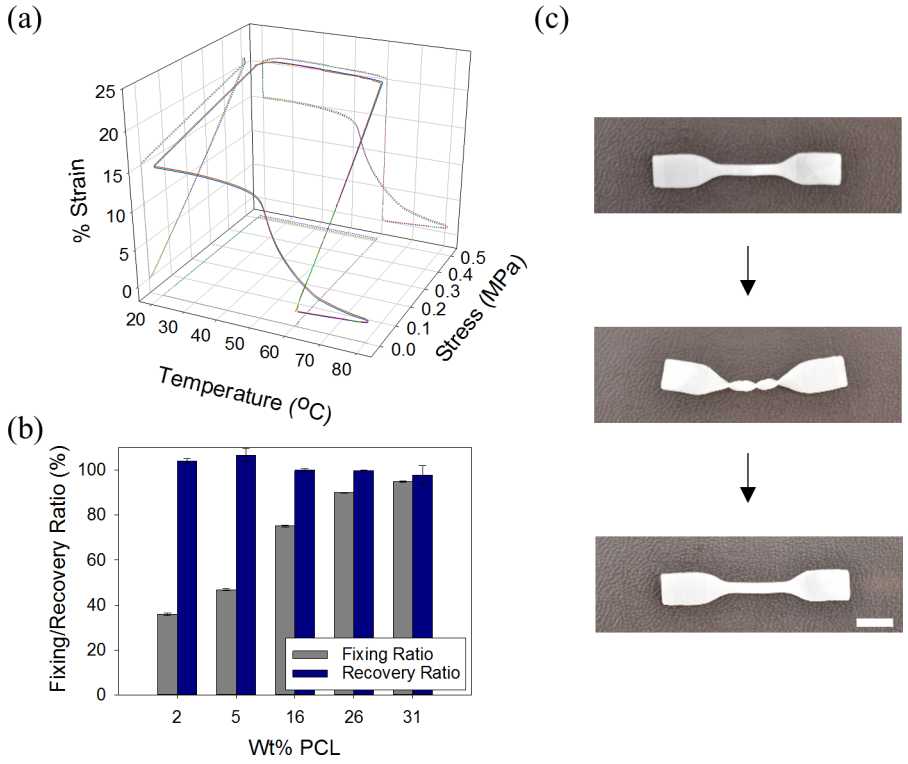

Figure 4. Shape memory characterization of the SMECs. (a) A representative 3D shape memory graph of stress, temperature, and strain for the SMEC containing 16 wt % PCL. (b) Fixing and recovery ratios for the SMECs with varying PCL content. (c) Images of a qualitative shape memory test, showing the initial flat dog bone shape of the SMEC (top), the fixed, temporary twisted shape (middle), and the recovered flat dog bone (bottom). The scale bar represents 5 mm for all images. Shape memory curves for all SMECs and a video of the qualitative shape memory test are available in the Supporting Information.

25 °C, the moduli of the SMECs were between 10 and 50 MPa, indicating the soft and elastomeric nature of the composites and more closely matching the moduli of human tissue[25−28] than typical SMPs (a table containing storage modulus values at 25 °C and a more complete mechanical characterization, including stress−strain curves and an elasticity test, are provided in the Supporting Information). At around 50 °C, the PCL melted, and the sample storage modulus dropped below detection in the DMA. At the same temperature, the SMECs dropped in storage modulus but reached a rubbery plateau, since the Pellethane fibers, still below their T_m, gave integrity to the films and prevented them from flowing as liquids.

Due to the presence of the rubbery plateau above PCL's T_m, we expected that the SMEC films would exhibit SM properties.[29] A three-dimensional stress-temperature-strain plot was prepared (Figure 4a), showing the response of a SMEC to the SM cycle (for experimental details of the SM cycle, see the Experimental Section). The shape fixing, characterized by the fixing ratio[21] (Figure 4b), which quantifies how much of the programmed deformation is maintained upon unloading, generally increased with increasing PCL content. This was expected since shape fixing relies on PCL crystallization and competes with the Pellethane's elasticity. Further, the recovery ratios[21] (Figure 4b) were greater than 97% (averaged over three cycles) for all compositions. In some cases, the recovery ratios were over 100%. We expect this is due to the recovery of residual stresses imparted during the compression molding process. Compared to blended SMECs prepared via solvent casting, for example, the dual-spun SMECs exhibited higher fixing and recovery ratios (fixing and recovery ratios for blended SMECs are provided in the Supporting Information). We attribute the improved fixing and recovery to the discrete and homogeneously distributed PCL and Pellethane phases. Furthermore, the homogeneity of the dual-spun SMECs leads to a reliability in performance not achieved with the blended SMECs. Images of a qualitative SM test can be seen in Figure 4c. A SMEC strip was fixed into a temporary twisted shape and recovered by heating above PCL's T_m. A video of the qualitative SM test is available in the Supporting Information. The consistency in performance and the high shape fixity and recovery of the SMECs make these materials promising candidates for soft SMP applications.

In this communication, we have presented a new approach to fabricate SMECs. The fully thermoplastic system allows for dual-electrospinning of both polymers. Advantages of this approach over previous SMEC fabrication methods include: the ability to tune the relative composition of the PCL and elastomer, which affects the mechanical properties of the material; the ease with which this process can be scaled to the industrial level, as the polymers are commercially available and the processing techniques are industrially relevant; and the added ability to redefine the permanent shape, since both polymers are thermoplastics. Further, the biocompatibility of the component polymers combined with the material properties of the composites make the SMECs relevant in the field of SM medical devices and SM rubbers.

EXPERIMENTAL METHODS

Materials. Poly(ε-caprolactone) (PCL), *N*,*N*-dimethylformamide (DMF), chloroform, and tetrahydrofuran were purchased from Sigma-

DOI: 10.1021/acsmacrolett.5b00106
ACS Macro Lett. 2015, 4, 436−440

Aldrich. Pellethane 5863−80A (Pellethane) was kindly supplied by Lubrizol Corporation. All materials were used as received.

Electrospinning. A 20% (w/v) PCL solution was prepared by dissolving 2 g PCL in 8 mL of chloroform and 2 mL of DMF. A 10% (w/v) Pellethane solution was prepared by dissolving 1 g Pellethane in 6 mL of THF and 4 mL of DMF. Flow rates varied between 0.2 and 0.6 mL h^{-1} for PCL and between 3.6 and 7.6 mL h^{-1} for Pellethane. The rates were chosen for each polymer so as to obtain the desired composition. The voltages applied to each needle were adjusted to accommodate the flow rates, with higher voltages applied for higher flow rates. The fibers were collected on a translating and rotating mandrel, and the tip of the needle to collector distances were maintained at about 8 cm for PCL and about 10 cm for Pellethane. Dual-electrospinning was chosen over other preparation methods, such as solvent casting or melt mixing, because of its ability to uniformly distribute two immiscible polymers.

Microscopy. To visualize the dual-spun fibers and the film surfaces and cross sections, a JEOL JSM-5600 scanning electron microscope (SEM) was used with a typical accelerating voltage of 6−8 kV. All samples were gold sputtered for 45 s prior to imaging.

Differential Scanning Calorimetry. A TA Instruments Q200 differential scanning calorimeter (DSC) was used to measure the transition temperatures and enthalpies of melting associated with melt transitions. All samples were first cooled to −80 °C, heated at 10 °C min^{-1} to 200 °C, cooled at 10 °C min^{-1} to −80 °C, and then heated 10 °C min^{-1} to 200 °C. The second heating cycles were studied to eliminate effects from different thermal histories. The glass and melt transition temperatures were chosen as the middle point of the step transition and the melting peak transition, respectively.

Wide Angle X-ray Scattering. A Rigaku generator (MicroMax-002+) was used with an accelerating voltage of 45 kV and a current of 0.88 mA to produce X-rays with a wavelength of 1.5405 Å. Under vacuum, samples were exposed to radiation for 1 h. The detector distance was fixed at 122.7, resulting in scatter angles in the range of $0° < 2\theta < 40°$. A FujiFilm FLA7000 reader was used to collect the scattered X-ray diffraction patterns, and SAXSgui software was used for analysis.

Dynamic Mechanical Analysis. A TA Instruments Q800 dynamic mechanical analyzer (DMA) was used to compare the moduli of the SMEC films with different compositions. The DMA was used in multifrequency strain mode, and each film was quenched at −70 °C, held isothermal for 10 min, and then heated at 3 °C min^{-1} to 160 °C. An oscillation amplitude of 15 μm, a preload force of 0.001 N, and a force track of 108% were used. Dog bone (ASTM D63 Type IV, scaled down by a factor of 4) shaped samples, with typical thicknesses of 0.6 mm, were used for testing.

Tensile mechanical testing. A Test Resources mechanical tester with a 100 lb (444.8 N) load cell was used to generate stress−strain curves for the SMEC films with varying PCL content. Dog bone (ASTM D63 Type IV, scaled down by a factor of 4) shaped samples were stretched at RT at 33 μm s^{-1} to failure. Young's modulus values were obtained from the slope of the stress−strain curve in the linear elastic region.

Elasticity Testing. A TA Instruments AR G2 Rheometer was employed in a tensile mode to determine the elasticity of a dog bone (ASTM D63 Type IV, scaled down by a factor of 4) shaped 16 wt % PCL SMEC film. The sample was stretched to 100% strain at 33 μm s^{-1} at RT. Immediately after reaching 100% strain, the sample was unloaded at 33 μm s^{-1}. This cycle was repeated two times, and the elasticity ratio (R_e) of each cycle was calculated using the equation,

$$R_e(\%) = \frac{\varepsilon_d - \varepsilon_u}{\varepsilon_d - \varepsilon_i} \quad (1)$$

where ε_d is the deformed strain prior to unloading, ε_u is the strain at 0 stress after unloading, and ε_i is the initial strain at the beginning of the cycle.

Shape Memory Testing. Using the DMA in controlled force mode, dog bone (ASTM D63 Type IV, scaled down by a factor of 4) shaped SMEC films were stretched at 60 °C to 20% strain by ramping the force at 0.02 N min^{-1}. The temperature was then ramped at 3 °C min^{-1} to 20 °C and held isothermal for 10 min to fix the temporary shape. The force was then unloaded at 0.05 N min^{-1} to the preload force, 0.001 N. To recover the permanent shape, the SMECs were heated at 3 °C min^{-1} to 80 °C, held isothermal for 5 min, and then cooled back to 60 °C at 3 °C min^{-1}. This cycle was repeated two times to yield a three-cycle SM program. The fixing (R_f) and recovery (R_r) ratios were calculated for each cycle using the following equations:

$$R_f(\%) = \frac{\varepsilon_f - \varepsilon_i}{\varepsilon_d - \varepsilon_i} \times 100 \quad (2)$$

$$R_r(\%) = \frac{\varepsilon_f - \varepsilon_r}{\varepsilon_f - \varepsilon_i} \times 100 \quad (3)$$

where ε_f is the fixed strain after unloading and ε_r is the recovered strain after heating.

Blended SMEC Fabrication. Blended SMECs were prepared via solvent casting and compression molding for comparison to the dual-spun SMECs. PCL and Pellethane were dissolved in a 60:40 THF/DMF volume ratio solution to obtain a 10% (w/v) solution. The relative weight fractions of PCL and Pellethane were varied to match the compositions prepared via dual-electrospinning. To ensure complete dissolution and mixing of both polymers, the solution was stirred overnight at RT. Once completely mixed, the solution was poured into a Teflon dish, and the solvent was allowed to evaporate for 2 days. The blended polymer film was dried in a RT vacuum oven (ca. 760 mmHg) overnight to remove any residual solvent. For better comparison to the dual-spun SMECs and to improve the uniformity of the films, the solvent cast PCL/Pellethane films were subsequently compression molded at 160 °C for 15 min under 1 t applied load.

Qualitative shape memory testing. A dog bone (ASTM D63 Type IV, scaled down by a factor of 4) shaped sample was first heated in warm water ($T > 56$ °C) to melt the PCL. Using forceps, the sample was twisted 4 full rotations and submerged in ice water for several seconds to crystallize the PCL and fix the temporary shape. The fixed twist was then submerged, again, in the warm water to melt the PCL and allow for recovery of the permanent shape. Images were taken between each step (Figure 4c), and a video (available in the Supporting Information) was taken to emphasize the fast and complete recovery of the SMECs when heated above PCL's T_m.

■ ASSOCIATED CONTENT

Supporting Information

Figures (1) Scanning electron microscopy images of all SMEC compositions, (2) differential scanning calorimetry second heating curve of neat Pellethane, (3) wide-angle X-ray scattering analysis of PCL, Pellethane, and the SMECs, (4) loss tangent curves for PCL, Pellethane, and the SMECs, (5) stress-strain curves for PCL, Pellethane, and the SMECs, (6) elasticity test of a SMEC film with 16 wt % PCL, (7) shape memory stress-temperature-strain plots for all SMEC compositions, (8) fixing and recovery ratios of the dual-spun and blended SMECs; (s) video of a qualitative shape memory test; Table (1) summary of the thermomechanical properties of PCL, Pellethane, and the SMECs. This material is available free of charge via the Internet at http://pubs.acs.org.

■ AUTHOR INFORMATION

Corresponding Author

*E-mail: ptmather@syr.edu. Tel.: (315) 443-8760. Fax: (315) 443-9175.

Notes

The authors declare no competing financial interest.

■ ACKNOWLEDGMENTS

P.T.M. acknowledges funding for this work under NSF CMMI-1334658 and NSF EFRI-1435452.

DOI: 10.1021/acsmacrolett.5b00106
ACS Macro Lett. 2015, 4, 436−440

REFERENCES

(1) Lendlein, A.; Kelch, S. *Angew. Chem., Int. Ed.* **2002**, *41* (12), 2034−2057.
(2) Mather, P. T.; Luo, X.; Rousseau, I. A. *Annu. Rev. Mater. Res.* **2009**, *39* (1), 445−471.
(3) Torbati, A. H.; Nejad, H. B.; Ponce, M.; Sutton, J. P.; Mather, P. T. *Soft Matter* **2014**, *10* (17), 3112−3121.
(4) Santiago, D.; Ferrando, F.; De la Flor, S. *J. Mater. Eng. Perform.* **2014**, *23* (7), 2567−2573.
(5) Westbrook, K. K.; Mather, P. T.; Parakh, V.; Dunn, M. L.; Ge, Q.; Lee, B. M.; Qi, H. J. *Smart Mater. Struct.* **2011**, *20* (6), 065010.
(6) Nejad, H. B.; Baker, R. M.; Mather, P. T. *Soft Matter* **2014**, *10* (40), 8066−8074.
(7) Lv, H.; Leng, J.; Liu, Y.; Du, S. *Adv. Eng. Mater.* **2008**, *10* (6), 592−595.
(8) Huang, W. M.; Yang, B.; An, L.; Li, C.; Chan, Y. S. *Appl. Phys. Lett.* **2005**, *86* (11), -.
(9) Gu, X.; Mather, P. T. *RSC Adv.* **2013**, *3* (36), 15783−15791.
(10) Luo, X.; Mather, P. T. *Soft Matter* **2010**, *6* (10), 2146−2149.
(11) Leng, J. S.; Lan, X.; Liu, Y. J.; Du, S. Y.; Huang, W. M.; Liu, N.; Phee, S. J.; Yuan, Q. *Appl. Phys. Lett.* **2008**, *92* (1).
(12) Lendlein, A.; Jiang, H.; Junger, O.; Langer, R. *Nature* **2005**, *434* (7035), 879−882.
(13) Lee, K. M.; Koerner, H.; Vaia, R. A.; Bunning, T. J.; White, T. J. *Soft Matter* **2011**, *7* (9), 4318−4324.
(14) Long, K. N.; Scott, T. F.; Jerry, Q. H.; Bowman, C. N.; Dunn, M. L. *J. Mech. Phys. Solids* **2009**, *57* (7), 1103−1121.
(15) Schmidt, A. M. *Macromol. Rapid Commun.* **2006**, *27* (14), 1168−1172.
(16) Buckley, P. R.; McKinley, G. H.; Wilson, T. S.; Small, W.; Benett, W. J.; Bearinger, J. P.; McElfresh, M. W.; Maitland, D. J. *IEEE Trans. Biomed. Eng.* **2006**, *53* (10), 2075−2083.
(17) Mohr, R.; Kratz, K.; Weigel, T.; Lucka-Gabor, M.; Moneke, M.; Lendlein, A. *Proc. Natl. Acad. Sci. U.S.A.* **2006**, *103* (10), 3540−3545.
(18) Chen, H.; Li, Y.; Liu, Y.; Gong, T.; Wang, L.; Zhou, S. *Polym. Chem.* **2014**, *5* (17), 5168−5174.
(19) Han, X.-J. H.; Dong, Z.-Q.; Fan, M.-M.; Liu, Y.; Li, J.-H.; Wang, Y.-F.; Yuan, Q.-J.; Li, B.-J.; Zhang, S. *Macromol. Rapid Commun.* **2012**, *33* (12), 1055−1060.
(20) Ge, Q.; Luo, X.; Iversen, C. B.; Nejad, H. B.; Mather, P. T.; Dunn, M. L.; Jerry, Q. H. *Int. J. Solids Struct.* **2014**, *51* (15−16), 2777−2790.
(21) Luo, X.; Mather, P. T. *Macromolecules* **2009**, *42* (19), 7251−7253.
(22) Ding, B.; Kimura, E.; Sato, T.; Fujita, S.; Shiratori, S. *Polymer* **2004**, *45* (6), 1895−1902.
(23) Varesano, A.; Carletto, R. A.; Mazzuchetti, G. *J.Mater. Process. Technol.* **2009**, *209* (11), 5178−5185.
(24) Bonk, H. W.; Sardanopoli, A. A.; Ulrich, H.; Sayigh, A. A. R. *J. Elastomers Plast.* **1971**, *3* (3), 157−186.
(25) Saraf, H.; Ramesh, K. T.; Lennon, A. M.; Merkle, A. C.; Roberts, J. C. *J. Biomech.* **2007**, *40* (9), 1960−1967.
(26) Roeder, B. A.; Kokini, K.; Sturgis, J. E.; Robinson, J. P.; Voytik-Harbin, S. L. *J. Biomech. Eng.* **2002**, *124* (2), 214−222.
(27) Mavrilas, D.; Sinouris, E. A.; Vynios, D. H.; Papageorgakopoulou, N. *J. Biomech.* **2005**, *38* (4), 761−768.
(28) Fung, Y. C. *Biomechanics: Motion, Flow, Stress, and Growth*; Springer-Verlag: New York, 1990.
(29) Liu, C.; Qin, H.; Mather, P. T. *J. Mater. Chem.* **2007**, *17* (16), 1543−1558.

DOI: 10.1021/acsmacrolett.5b00106
ACS Macro Lett. 2015, 4, 436−440